Far-Infrared Spectrum and Hindering Potential of Deuterium Peroxide

ROBERT H. HUNT
Department of Physics, The Florida State University, Tallahassee, Florida
AND
ROBERT A. LEACOCK*
The Harrison M. Randall Laboratory of Physics, The University of Michigan, Ann Arbor, Michigan
(Received 17 June 1966)

The hindered-rotation motion in the deuterium peroxide molecule is investigated through a study of the far-infrared absorption of the vapor. A 1-m focal-length vacuum grating spectrometer was used to scan the region from 20 to 400 cm^{-1} with an average resolution of 0.4 cm^{-1}. Seven perpendicular-type hindered-rotation bands characterized by prominent Q branches and unresolved P- and R-branch structure are observed in the spectrum. The band centers are located at 1.88, 42.3, 123.5, 136.8, 206.7, 250.9, and 302.6 cm^{-1}. From these it is determined that, relative to the ground state, the first five excited hindered-rotation states are at 1.88, 208.6, 250.9, 387.7, and 511.2 cm^{-1}.

A theory of internal rotation, developed for an earlier application to the far-infrared spectrum of hydrogen peroxide, is applied to the D_2O_2 spectrum. In this theory the only internal degree of freedom is the dihedral angle x defining the relative position of the two OD groups. The Hamiltonian is put in the form H (asymmetric top) $+H$ (internal rotation), where the inertial coefficients are functions of the internal angle x. A three-parameter hindering potential is assumed, $V(x)=V_1\cos x+V_2\cos 2x+V_3\cos 3x$ and the internal-rotation wave equation is solved numerically by computer to obtain the potential parameters which reproduce the internal-rotation energy eigenvalues. In the semirigid model adopted, the effective hindering potentials, bond lengths, and bond angles of H_2O_2 and D_2O_2 differ slightly. The data do not yield a complete set of effective bond lengths and angles for D_2O_2, but the product of the OD distance and the sine of the OOD angle is found to be 0.01 Å smaller than its H_2O_2 counterpart. As a result, the inertial parameter in the internal-rotation wave equation is 2% larger than is predicted from the H_2O_2 data. Using this adjusted inertial parameter, the hindering potential $V(x)=994\cos x+641\cos 2x+55\cos 3x$ provides a good fit to the D_2O_2 data. For this potential function the *cis* and *trans* potential barrier heights are 2470 and 377 cm^{-1}, respectively, and the potential minima are 110.8° from the *cis* configuration. These parameter values are similar to the corresponding H_2O_2 values of 2460 cm^{-1}, 386 cm^{-1}, and 111.5°.

INTRODUCTION

IN an earlier paper[1] (hereafter referred to as I) a theory of hindered internal rotation was developed for the hydrogen peroxide molecule H_2O_2 and its deuterated forms D_2O_2 and HOOD. This theory was applied to the analysis of the far-infrared spectrum of H_2O_2 vapor and an effective hindering potential function was determined for that molecule. Only a limited study of D_2O_2 was possible at that time. Using the microwave data of Massey, Beard, and Jen,[2] it was shown in I that the first excited hindered-rotation state of D_2O_2 was split by about 41 cm^{-1}, and that such a splitting was consistent with that calculated using the H_2O_2 hindering potential.

This paper extends the treatment of D_2O_2 to include the results of a 0.4-cm^{-1} resolution study of its vapor absorption between 20 and 400 cm^{-1}. Analysis of this spectrum yields the D_2O_2 potential parameters, $V(cis)=2470$ cm^{-1}, $V(trans)=377$ cm^{-1} with a potential minimum x_0,* 110.8° from the *cis* configuration. These parameter values serve to confirm the spectral analysis of H_2O_2 in I as they differ only slightly from the corresponding H_2O_2 values: $V(cis)=2460$ cm^{-1}, $V(trans)=386$ cm^{-1} and $x_0=111.5°$. The present data do not uniquely determine the effective bond lengths and angles of D_2O_2. However, it is found that the product of the OD distance and the sine of the OOD angle is 0.01 Å smaller than its H_2O_2 counterpart.

EXPERIMENTAL

The spectra were obtained using the 1-m focal-length vacuum grating spectrometer and the aluminum and glass absorption cell described in I. The sample of D_2O_2, obtained from Giguère of Laval University, Quebec, Canada, was at the time of its preparation approximately 91% D_2O_2 and 8% D_2O. Static samples of D_2O_2 vapor decomposed too rapidly in the absorption cell to be of use and it was necessary to follow the continuous-flow procedure adopted for H_2O_2. D_2O_2 vapor from a liquid sample maintained at about 25°C was admitted to the cell at one end and was slowly and continuously withdrawn at the other end by a cold trap and vacuum pump. Pumping speeds sufficient to avoid strong absorption from the decomposition product D_2O were usually in the range of 1 to 2 ml/h. The 100-ml sample was sufficient to obtain two or more

* Present address: Department of Physics, Iowa State University, Ames, Ia.
[1] R. H. Hunt, R. A. Leacock, C. W. Peters, and K. T. Hecht, J. Chem. Phys. **42**, 1931 (1965).
[2] J. T. Massey, C. I. Beard, and C. K. Jen, J. Mol. Spectry. **5**, 405 (1960).

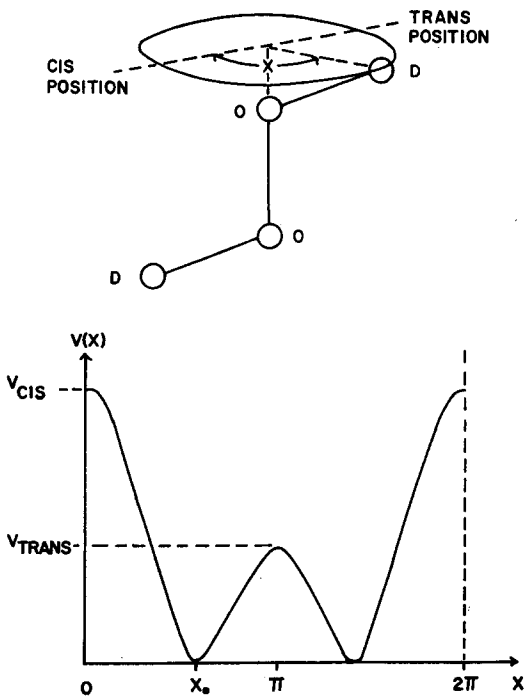

FIG. 1. The structure and hindering potential of D_2O_2.

runs over all portions of the 20- to 400-cm^{-1} region. The absorption of D_2O vapor between 20 and 400 cm^{-1} was also measured as a means of estimating the D_2O contamination of the D_2O_2 spectrum.

Absorption paths in the 0.4-m-long White cell ranged from 1.6 m between 20 and 300 cm^{-1} to 3.2 m between 300 and 400 cm^{-1}. Because the Golay cell detector suffered a loss in sensitivity at the beginning of this work, the average spectral slit width is 0.4 cm^{-1} as compared to the 0.3 cm^{-1} reported for H_2O_2.

THEORY

The theory of internal rotation in D_2O_2 is given in I. The results are summarized here. Figure 1 shows the structure of D_2O_2 and the form of the internal-rotation hindering potential. A semirigid model is adopted in which the only internal degree of freedom is the angle of relative internal rotation x. A set of molecular axes is chosen for which the Hamiltonian has the form [Eq. (3.4) in I]:

$$H=\beta(x)P^2+\nu(x)P_Z^2+\gamma(x)(P_X^2-P_Y^2)+\delta(x)(P_YP_Z+P_ZP_Y)+\alpha(x)p_x^2+V(x).$$

P is the total angular momentum with components P_X,[f] P_Y, and P_Z referred to the molecule-fixed axes X, Y, Z. p_x is the momentum conjugate to the internal-rotation angle x, and $V(x)$ is the internal-rotation potential-energy function.

The inertial coefficients $\beta(x)$, $\nu(x)$, $\delta(x)$, $\gamma(x)$, and $\alpha(x)$ are functions of the internal angle x, the OO and OD distances, and the OOD angles. The values of the latter three equivalent parameters in H_2O_2 as proposed by Redington, Olson, and Cross[3] and as adopted in I are: OO distance 1.475 Å, OH distance 0.950 Å, and OOH angle 94.8°.

Because these parameters are effective values for the vibrational ground state of H_2O_2 and contain implicit mass dependent contributions from vibration–rotation interactions, the corresponding parameters for D_2O_2 are slightly different. However, as remarked, the present data are not sufficient to determine them completely. For this reason the data for D_2O_2 are first compared with calculations based on the H_2O_2 parameters and the latter are then modified as required. Using the H_2O_2 bond lengths and angles, the following expansions of the inertial coefficients of D_2O_2 are obtained in cm^{-1} (see Appendix III of I):

$$\beta(x)=0.772+0.00692\cos x+0.00241\cos 2x+\cdots,$$

$$\nu(x)=4.598-0.135\cos x+0.0134\cos 2x+\cdots,$$

$$\gamma(x)=0.00184+0.0550\cos x+0.00098\cos 2x+\cdots,$$

$$\alpha(x)=21.277+0.190\cos x+0.0960\cos 2x+\cdots,$$

$$\delta(x)=0.146\sin^3\tfrac{1}{2}x+\cdots.$$

In lowest order, the Hamiltonian separates into that of a rigid symmetric top plus an internal-rotation Hamiltonian $\alpha(x)p_x^2+V(x)$. The eigenfunctions of the latter Hamiltonian are denoted by $M_{n\tau}(x)$. n is a principal quantum number ordering the internal-rotation energy levels of a given symmetry species τ. The symmetries of $M_{n\tau}$ under the operations σ_t and σ_c (reflections in the *trans* and *cis* planes, respectively) are given in Table I.

The hindering potential is assumed to have the form $V(x)=V_1\cos x+V_2\cos 2x+V_3\cos 3x$. The resulting Mathieu-type internal-rotation wave equation is solved by computer for appropriate values of the input parameters V_1, V_2, and V_3. The latter are chosen so that the calculated internal-rotation energy eigenvalues coincide with those determined from analysis of the far-infrared spectrum. The computer calculation also gives the internal-rotation eigenfunction $M_{n\tau}(x)$ and the matrix

TABLE I. Symmetry of the internal-rotation wavefunctions.

K value (even or odd)	Symmetry under σ_t	Symmetry under σ_c	τ quantum number
e	s	s	1
o	s	a	2
o	a	s	3
e	a	a	4

[3] R. L. Redington, W. B. Olson, and P. C. Cross, J. Chem. Phys. 36, 1311 (1962).

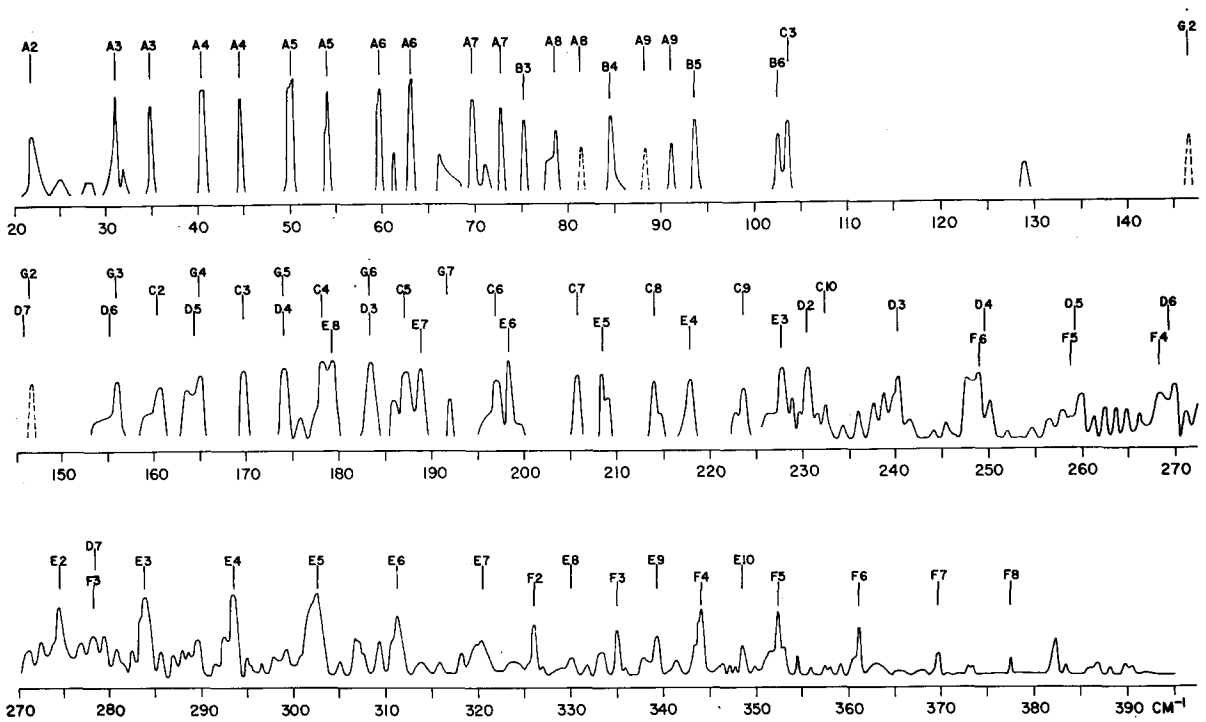

FIG. 2. The absorption spectrum of D_2O_2 vapor from 20 to 400 cm^{-1}.

elements of $\cos x$, $\cos 2x$, $\sin^3(\frac{1}{2}x)$, and $\cos(\frac{1}{2}x)$ for use in the perturbation-theory calculation.

The full Hamiltonian matrix is then written using the basis functions

$$\psi_{J(K\pm)Mn\tau}=1\sqrt{2}(\psi_{JKM}\pm\psi_{J(-K)M})M_{n\tau}$$

$$\psi_{JOMn\tau}=\psi_{JOM}M_{n\tau},$$

where the ψ_{JKM} are the symmetric-top wavefunctions. Since the off-diagonal (in K) matrix elements of the full Hamiltonian are small, the energy levels of the semirigid model of the molecule can be calculated to an accuracy of several hundredths of a wavenumber using second-order perturbation theory.

The zeroth-order selection rules for hindered-rotation transitions are discussed in I and are summarized here in Table II.

RESULTS

The absorption spectrum of D_2O_2 vapor between 20 and 400 cm^{-1} is shown in Fig. 2. In some regions the weaker absorption lines have been omitted because of the difficulty in distinguishing the contribution from D_2O. Dashed portions of the spectrum indicate where moderately strong lines of D_2O and D_2O_2 overlap, rendering the intensity of the latter quite uncertain.

There is no strong evidence for HOOD, H_2O, or HDO absorption arising from the sample. Some spectra did show the strongest rotational lines of H_2O to a slight extent, but these were due to the modest vacuum attainable in the source housing. The spectrum of D_2O, run for comparison purposes, is in good agreement with that of Fuson, Randall, and Dennison.[4]

Table III lists the frequencies of the major absorption lines of D_2O_2 vapor measured at the absorption peaks. The estimated error in the measurement of well-defined absorption peaks is ± 0.05 cm^{-1}. A comparison of the peak percent absorption for the same path length is also given.

As in the case of H_2O_2, the hindered-rotation bands of D_2O_2 are perpendicular in character with prominent Q branches (except near the band centers) and unresolved P- and R-branch structure. Seven such bands have been identified. They are analyzed using the positions of the Q-branch absorption peaks as approximate Q-subband heads. The positions of the latter in the $n\tau\rightarrow n'\tau'$ hindered-rotation band are then fitted

TABLE II. Selection rules for hindered-rotation bands of D_2O_2.

$\Delta J=0$ transitions	$\Delta J=\pm 1$ transitions
$(K+)\rightarrow(K+)\pm 1$	$(K+)\rightarrow(K-)\pm 1$
$(K-)\rightarrow(K-)\pm 1$	$(K-)\rightarrow(K+)\pm 1$
$n\rightarrow n'$	$n\rightarrow n'$
$\tau=1\rightarrow 3$ or $=2\rightarrow 4$	$\tau=1\rightarrow 3$ or $=2\rightarrow 4$

[4] N. Fuson, H. M. Randall, and D. M. Dennison, Phys. Rev. 56, 982 (1939).

TABLE III. Frequencies of the principal absorption lines of D_2O_2 vapor between 20 and 400 cm^{-1}.

Frequency (cm^{-1})	Percent absorption	Frequency (cm^{-1})	Percent absorption	Frequency (cm^{-1})	Percent absorption
21.83	35	169.68	40	269.71	30
31.24	55	173.81	40	274.83	35
34.97	50	178.42	45	278.23	20
40.66	55	179.30	45	279.47	20
44.46	50	183.22	45	283.89	40
50.24	60	186.30	20	293.35	40
53.90	55	187.52	35	302.60	40
59.71	55	188.84	40	307.02	20
63.32	65	191.88	20	309.20	20
69.13	50	196.47	30	311.78	30
72.62	45	198.33	45	320.6	20
75.27	40	205.56	35	325.99	25
78.57	35	208.0	35	330.13	10
84.35	45	214.34	30	333.5	15
91.31	30	217.69	30	334.95	25
93.63	40	223.55	25	339.23	20
102.51	35	227.42	35	343.60	35
103.52	40	230.78	35	348.44	15
129.22	15	232.19	15	352.46	35
146.6	...	240.23	30	360.90	25
155.78	35	248.0	...	369.29	15
160.59	30	250.17	20	377.43	10
163.8	25	259.90	25	382.59	20
165.00	35	268.75	25		

to the equation

$$Q_K(0) = \nu_{n'\tau'}{}^{n'\tau'}(K\pm1)^2 - \nu_{n\tau}{}^{n\tau}K^2 + E_{n'\tau'} - E_{n\tau} - D_K[(K\pm1)^4 - K^4]$$

using combination relations wherever possible. D_K is a distortion coefficient added empirically to include vibration–over-all-rotation interactions. The upper sign applies to ${}^RQ_K$ branches, the lower sign to ${}^PQ_K$ branches. $E_{n\tau}$ is the energy of the $n\tau$ internal-rotation state and the rotational constant $\nu_{n\tau}{}^{n\tau}$ is the expectation value of $\nu(x)$ in that state.

Table IV lists the hindered-rotation band centers obtained and the internal-rotation transitions from which they arise. The errors quoted for the band centers are based on the analyses of the individual bands except for Bands *D* and *G*. The centers of these bands are more precisely determined from the energy-level positions obtained from the other bands.

Experimental values for $\nu_{n\tau}{}^{n\tau}$ are given in Table V along with a value for D_K.

TABLE IV. Observed D_2O_2 band centers and band assignments.

	Band center (in cm^{-1})	Internal-rotation transition $n\tau \rightarrow n'\tau'$
A	1.88±0.06	01→03, 02→04
B	42.3 ±0.2	11→13, 12→14
C	136.8 ±0.2	13→21, 14→22
D	206.7 ±0.3	03→11, 04→12
E	250.9 ±0.1	01→13, 02→14
F	302.6 ±0.3	11→23, 12→24
G	123.5 ±0.3	21→23, 22→24

Figure 3 compares the observed D_2O_2 internal-rotation energy-level scheme with that calculated from the bond constants and hindering potential of H_2O_2. The letters labeling the internal-rotation transitions correspond to the letters of Fig. 2 and Table IV. Several matrix elements calculated with the H_2O_2 potential are given in Table VI. Comparison of Tables V and VI and inspection of Fig. 3 reveals that the effective hindering potentials and bond constants of H_2O_2 and D_2O_2 differ only slightly.

Absence of experimental values for $\gamma_{n\tau}{}^{n\tau}$ and $\beta_{n\tau}{}^{n\tau}$ prevents a unique determination of the OO and OD distances and the OOD angle. However, since $\nu_{01}{}^{01}$ as calculated from H_2O_2 data is 0.094 cm^{-1} smaller than the experimental value of 4.742 cm^{-1}, it follows that the product of the OD distance and the sine of the OOD angle is 0.936±0.006 Å, i.e., 0.01 Å smaller than its H_2O_2 counterpart. This is because $\nu(x)$, in first approximation, varies as the inverse square of the above product and depends only weakly on other functions of the bond constants. This is also true of $\alpha(x)$, the inertial coefficient in the internal-rotation wave equation. As a result, α_0, the major term in $\alpha(x)$, has an

TABLE V. Experimental values of $\nu_{n\tau}{}^{n\tau}$ for $n=0, 1, 2$.

$\nu_{01}{}^{01} = \nu_{02}{}^{02} = 4.742\pm0.002$ cm^{-1}
$\nu_{03}{}^{03} = \nu_{04}{}^{04} = 4.740\pm0.002$
$\nu_{11}{}^{11} = \nu_{12}{}^{12} = 4.76\pm0.01$
$\nu_{13}{}^{13} = \nu_{14}{}^{14} = 4.730\pm0.005$
$\nu_{21}{}^{21} = \nu_{22}{}^{22} = 4.70\pm0.01$
$\nu_{23}{}^{23} = \nu_{24}{}^{24} = 4.69\pm0.02$

$D_K = (1.3\pm0.2)\times10^{-4}$ cm^{-1} for all bands.

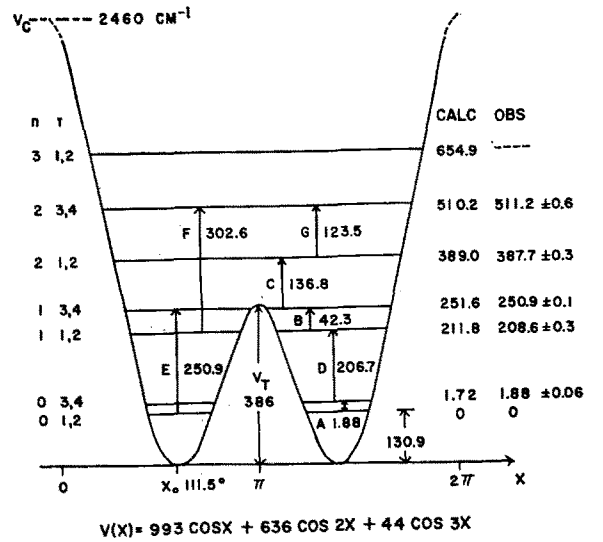

FIG. 3. Comparison of the observed D_2O_2 internal-rotation energy levels with those calculated using the H_2O_2 hindering potential function and bond parameters.

effective value in D_2O_2 of 21.7±0.1 cm^{-1} as compared with the value of 21.3 cm^{-1} calculated from H_2O_2 data. The best fit to the experimental level positions based on this increased value of α_0 is then obtained with the D_2O_2 hindering potential function $V(x)=994\ \cos x+641\ \cos 2x+55\ \cos 3x$. This potential is characterized by

$$V(trans)=377\ \text{cm}^{-1},$$
$$V(cis)=2470\ \text{cm}^{-1},$$
$$x_0=110.8°.$$

The first five eigenvalues above the ground state calculated with this potential are 1.86, 208.7, 251.0, 387.1, and 510.7 cm^{-1} in good agreement with the experimental values. The ground state is 130.7 cm^{-1} above the potential minimum.

DISCUSSION

The 1.88-cm^{-1} band, whose Q branches are labeled A in Fig. 2, is well fitted by a perpendicular band analysis and it is from this band that D_K is determined. Table VII shows the observed Q-branch frequencies for this band and the same frequencies calculated using the constants of Tables IV and V. Table VIII gives similar comparisons for the remaining bands. The Q branches of these bands are identified in Fig. 2 by the same letter used to label the bands in Fig. 3 and by a number corresponding to the initial K value involved.

TABLE VI. Some computed matrix elements of D_2O_2 based on H_2O_2 parameters.

$n\tau$	$\beta_{n\tau}^{n\tau}$ (cm^{-1})	$\nu_{n\tau}^{n\tau}$	$\gamma_{n\tau}^{n\tau}$
01, 02	0.7681	4.648	−0.0220
03, 04	0.7681	4.646	−0.0213
11, 12	0.7681	4.685	−0.0330
13, 14	0.7684	4.658	−0.0242
21, 22	0.7686	4.670	−0.0274
23, 24	0.7690	4.650	−0.0205

TABLE VII. Calculated and observed Q-branch frequencies of the 1.88-cm^{-1} band.

	$n\tau$=01→03, 02→04		$n\tau$=03→01, 04→02	
K	Calc	Obs	Calc	Obs (cm^{-1})
2→3	25.56	•••	21.83	21.83
3→4	35.02	34.97	31.31	31.24
4→5	44.46	44.46	40.78	40.66
5→6	53.88	53.90	50.24	50.24
6→7	63.28	63.32	59.69	59.71
7→8	72.66	72.62	69.13	69.13
8→9	82.01	a	78.54	78.57
9→10	91.33	91.31	87.93	a

[a] Largely obscured by D_2O.

A relatively large number of absorption lines have been assigned to Q branches of the 250.9-cm^{-1} band. Assuming these assignments are correct, it is not understood why ${}^RQ_8$ appears much weaker than ${}^RQ_9$. ${}^RQ_{11}$ is the first Q branch which might be affected by a resonance arising from the Hamiltonian term

$$\gamma(x)(P_X^2-P_Y^2).$$

No ${}^PQ$ branches of the 302.6 cm^{-1} band, except possibly ${}^PQ_4$, can be identified with great certainty. They appear to be overlapped by the diffuse ${}^RQ_K$ branches of the much stronger 206.7-cm^{-1} band. Also, ${}^RQ_0$, ${}^PQ_1$, etc., of the 250.9-cm^{-1} band must contribute a considerable background of absorption in this region.

Series I of the microwave spectrum of Massey, Beard, and Jen[2] was ascribed in I to the transitions J, $(K\pm)$, n, $\tau=J$, $(4\pm)$, 1, 4→J, $(5\pm)$, 1, 2. This assignment is confirmed here by the observation of several other Q branches of this band which is centered at 42.3 cm^{-1}. In I this band was placed at 41.1 cm^{-1}. This number was based on values of $\nu_{n\tau}^{n\tau}$ calculated from H_2O_2 data which, as a comparison of Tables V and VI shows, are somewhat smaller than the experimental values. The head of this microwave series occurs at 1.28 cm^{-1}. The value calculated from the present data is 0.97 cm^{-1}. The errors quoted for the band constants are sufficient to encompass this difference, part of which may be due to the approximation of taking the observed absorption peaks as the Q-subband heads.

The 136.8-cm^{-1} band is well behaved. At this low frequency the asymmetry in the intensity distribution is quite pronounced.

The bands discussed above place the transition $n\tau$=21→23 at 123.5±0.3 cm^{-1}, and the transition

TABLE VIII. Calculated and observed Q-branch frequencies for six hindered-rotation bands.

Q branch	250.9 band (E)		136.8 band (C)		42.3 band (B)		302.6 band (F)		123.5 band (G)		206.7 band (D)	
	Calc	Obs	Calc	Obs	Calc	Obs	Calc	Obs	Calc[c]	Obs	Calc	Obs
$^RQ_{10}$	348.46	348.44	231.93	232.19 cm^{-1}								
$^RQ_9$	339.33	339.23	223.21	223.55								
$^RQ_8$	330.24	330.13	214.46	214.34			377.55	377.43	200.84	...		
$^RQ_7$	321.04	320.6	205.60	205.56	111.58	a	369.30	369.29	192.01	191.88	278.86	279.47
$^RQ_6$	311.82	311.78	196.68	196.47	102.57	102.51	360.91	360.90	183.12	183.22[d]	269.16	269.71
$^RQ_5$	302.55	302.60	187.67	187.52	93.50	93.63	352.35	352.46	174.14	173.81[d]	259.47	259.90
$^RQ_4$	293.23	293.35	178.57	178.42	84.34	84.35	343.64	343.60	165.09	165.00[d]	249.87	250.17
$^RQ_3$	283.88	283.89	169.41	169.68[d]	75.12	75.27	334.78	334.95	155.97	155.78[d]	240.18	240.23
$^RQ_2$	274.49	274.83	160.17	160.59	65.82	...	325.76	325.99	146.77	146.6[d]	230.57	230.78
$^PQ_3$	227.15	227.42	113.04	a			278.53	278.23	99.84	...	183.09	183.22[d]
$^PQ_4$	217.62	217.69	104.44	103.52			268.67	268.75	90.28	...	173.72	173.81[d]
$^PQ_5$	208.08	208.0	93.80	93.63[d]	−0.97	−1.28[b]	258.70	...			164.41	165.00[d]
$^PQ_6$	198.53	198.33					248.58	...			155.15	155.78[d]
$^PQ_7$	188.94	188.84									145.94	146.6[d]
$^PQ_8$	179.40	179.30										
$^PQ_9$	169.84	169.68[d]										

[a] Presence uncertain, D_2O strong here.
[b] Microwave value of Massey, Beard, and Jen.[3]
[c] Calculated using $\nu_{21}{}^{21}=4.71$, $\nu_{23}{}^{23}=4.68$.
[d] Absorptions common to two bands.

$n\tau = 03 \rightarrow 11$ at 206.7 ± 0.3 cm^{-1}. With the exception of ${}^{R}Q_2$, and possibly ${}^{R}Q_3$, the absorptions attributed in Table VIII to the ${}^{R}Q_K$ branches of the 206.7 band appear quite diffuse. Such diffuseness was characteristic of both the higher ${}^{R}Q_K$ and ${}^{P}Q_K$ branches of the analogous band in H_2O_2. If this is true for the ${}^{P}Q_K$ branches here, then the absorption lines at 165.0, 155.8, and 146.6 cm^{-1} are due largely to the 123.5-cm^{-1} band. As Table VIII shows, a good fit to this band is obtained if the values $\nu_{21}{}^{21} = 4.71$ cm^{-1} and $\nu_{23}{}^{23} = 4.68$ cm^{-1} are adopted. However, if $\nu_{11}{}^{11}$ is adjusted to 4.77 cm^{-1}, the three lines in question also fit the 206.7-cm^{-1} band reasonably well. Since such adjustments of the rotational constants are within their experimental errors, it is uncertain which band is the major contributor to these lines and it is also likely that these two bands combine to produce the absorption lines at 173.8 and 183.2 cm^{-1}. The line at 191.9 cm^{-1} assigned to ${}^{R}Q_7$ of the 123.5-cm^{-1} band is not considered to be decisive in the above argument.

Tables VII and VIII show that the agreement between observed and calculated Q-branch frequencies is generally poorest for the ${}^{R}Q_2$ and ${}^{P}Q_3$ branches and that, in some cases, these Q branches cannot be identified in the spectrum. In the present notation, these Q branches arise from the transitions $J, K+ = J, 2+ \leftrightarrow J, 3+$ and $J, K- = J, 2- \leftrightarrow J, 3-$. Calculations using the matrix elements of Table VI show that the first of these transitions is generally strongly J dependent, while the latter is moderately so. Because of unknown vibration–rotation interactions it is difficult to predict which of these Q branches should be observed. However, the following transitions should be spread over several wavenumbers since they all have quartic J coefficients calculated to be greater than 9×10^{-6} cm^{-1}: All of the $J, 2+ \rightarrow J, 3+$ transitions except those of the 206.7-cm^{-1} band, and all of the $J, 3+ \rightarrow J, 2+$ transitions except those of the 123.5- and 302.6-cm^{-1} bands. Thus, in those cases where ${}^{P}Q_3$ and ${}^{R}Q_2$ branches are observed, the contributing component, with the above exceptions, must be largely the $J, 2- \leftrightarrow J, 3-$ transitions. This explains why some of these Q branches appear to be of lower intensity than the neighboring ${}^{R}Q_3$ or ${}^{P}Q_4$ branches.

In H_2O_2 several Q branches involving $K=1$ were accidentally quite narrow. In D_2O_2 the constants are such that this does not occur.

ACKNOWLEDGMENTS

The authors would like to thank Professor Karl T. Hecht for valuable discussions and Professor Paul A. Giguère for the preparation of the D_2O_2 sample.